Engineering with Computers
https://doi.org/10.1007/s00366-018-0593-7

ORIGINAL ARTICLE

Adaptive analysis of plates and laminates using natural neighbor Galerkin meshless method

Basant Kumar[1,3] · **Madhukar Somireddy**[2] · **Amirtham Rajagopal**[3]

Received: 4 January 2018 / Accepted: 9 February 2018

Abstract
In this paper, natural neighbor Galerkin meshless method is employed for adaptive analysis of plates and laminates. The displacement field and strain field of plate are based on Reissner–Mindlin plate theory. The interpolation functions employed here were developed by Sibson and based on natural neighbor coordinates. An adaptive refinement strategy based on recovery energy norm which is in turn based on natural neighbors is employed for analysis of plates. The present adaptive procedure is applied to classical plate problems subjected to in-plane loads. In addition to that the laminated composite plates with cutouts subjected to transverse loads are investigated. Influence of the location of the cutout and the boundary conditions of the plate on the results have been studied. The results obtained with present adaptive analysis are accurate at lower computational effort when compare to that of no adaptivity. Further, the adaptive analysis provided accurate magnitude of maximum stresses and their locations in the laminate plates with and without cutout subjected to transverse loads. Additionally, failure prone areas in the geometry of the plates subjected to loads are revealed with the adaptive analysis.

Keywords Meshless methods · Natural neighbors · Adaptive strategy · Laminates · Plate theory

1 Introduction

Laminated composite materials usage is increased in light weight structural applications such as aerospace structures because of theirs high strength to weight ratio. The structures can have cutouts to pass hydraulic, electrical lines and also to facilitate the fuel passage lines. In some cases, cutouts are created for optimal design of the structures. In few other cases, the cutouts are made in the parts to assemble with other mating parts of the structure, for example, the cutouts for windows and doors in the fuselage of airplane. The laminate structures with such cutouts subjected to different mechanical loads need utmost care during design and analysis. It is because the sudden change in the geometry of the structures and sharp edges of the cutouts would lead to stress singularities. These stress singularities in such areas would lead the crack initiation and then ultimate failure of the structure. Thus, the stresses in such regions of the structures are important to calculate precisely for effective design and analysis of the structures. Calculation of stresses at singularity areas using classical numerical methods is not efficient because of the finite elements but this can be overcome by the meshless methods.

The classical finite element method (FEM) has been used extensively for several decades in the analysis of structures and has been successfully implemented in commercial structural analysis packages. The element distortion is significant consideration in finite element analysis of the complex geometries having stress singularities and it affects the performance of the method. The accuracy of results by finite element method depends on element shape, size and mesh density. Modeling thin structures with large deformation, material with discontinuities and crack modeling which are dealt with classical finite element method involve complexities such as adaptive mesh refinement, distortion of element in coarse mesh. Furthermore, finite element meshing of structures is tedious work and time consuming. To overcome such problems, meshless techniques have been developed by various researchers [1–4]. However, these meshless methods

✉ Madhukar Somireddy
madhukar@yorku.ca

[1] Advanced Systems Laboratory, DRDO, Hyderabad, India

[2] Department of Mechanical Engineering, York University, Toronto, Canada

[3] Department of Civil Engineering, IIT Hyderabad, Hyderabad, India

Published online: 15 February 2018

have restrictions on the imposition of essential and natural boundary conditions because approximations made do not satisfy delta Kronecker property ($\phi_I(x_J) \neq \delta_{IJ}$). The other meshless technique to overcome this problem is natural element method (NEM) and was developed by Sambridge et al. [5], where the interpolation function is based on Sibson [6] natural neighbor coordinates. The natural element method was successfully applied to solid mechanics problems by Sukumar et al. [7]. The meshless method for the analysis of the laminated structures is an unexplored research area and has been gaining popularity in recent years. However, analysis of laminated composite structure using plate theories is well established. A classical plate theory based on the Kirchhoff assumption works better for thin plates. To account for shear deformation effects in thick plates, shear deformation plate theories were developed. The first-order shear deformation theories [8–13] may be considered as the starting step where uniform transverse shear strain has taken over the entire laminate thickness. As the actual variation over the laminate thickness is not uniform, it requires an arbitrary shear correction factor. Higher order shear deformation theories [14–18] were proposed to overcome this limitation. The plate theories [8–18] are defined as single layer plate theory where the transverse shear strain is continuous across the entire thickness, which leads to discontinuity in the variation of the transverse shear stresses at the layer interfaces.

The meshless methods for the analysis of the plates are becoming popular in recent times. The natural neighbor radial point interpolation method (NNRPIM) proposed by Dinis et al. [19, 20] is based on natural neighbor concept for nodal connectivity and radial point interpolators for interpolation functions. The NNRPIM was applied to analysis of thick and laminated plates based Reissner–Mindlin plate theory. Dinis et al. [21] proposed a 3D shell-like approach based on NNRPIM for analysis of the thin plate and shell structures. The proposed method in article [11] was extended to dynamic analysis of thin structures [22]. An unconstrained third order shear deformation theory proposed by Leung [23] is similar to Reddy's TSDT, but it allows presence of transverse shear strains on the top and bottom of the plate. The accuracy of the results by this method is better than TSDT and closer to 3D elasticity solutions. Dinis et al. [24] extended NNRPIM to the analysis of functionally graded plates based on unconstrained third order plate theory. The accuracy and convergence rate by this improved meshless method is higher, but at the cost of higher computational effort when compare to FEM. The natural neighbor Petrov–Galerkin method for analysis of plate problems was developed by Li et al. [25]. Analysis of laminated plates was carried using natural Galerkin method by Madhukar and Rajagopal [37]. However, literature on adaptive analysis of complex geometric laminated structures using meshless methods is limited. Therefore, detail investigation on adaptive analysis using meshless techniques needs exploration.

Analysis of structures subjected to large deformations using finite element methods requires adaptive strategy at stress singularity regions for accurate results. The mesh refinement of domain for adaptive strategy is based on error estimation and more details about error estimation available in Zienkiewicz and Taylor [26]. The residual based error estimator was initially introduced by Babuska and Rheinboldt [27], then the recovery based error estimator was developed by Zienkiewicz and Zhu [28]. Then research work was carried-out for improving the performance of the error estimator. The error estimation application has been extensively applied for the analysis of engineering problems using FEM. The error estimation in bending analysis of laminated composite plate was carried by Mohite and Upadhyay [29–32]. Recently the same authors [38] investigated the optimization of laminate plates with cutouts based on the adaptive finite element method. A review on various available error estimators for the adaptive finite element analysis of the fracture mechanics problems and also goal-oriented error estimator for nonlinear analysis of structure are made available by Stein et al. [39, 40]. Rüter and Stein [41] presented goal-oriented adaptive strategies for the error calculation in linear elastic fracture mechanics problems. The mesh based computational method, finite element method, faces problems in refinement such as element compatibility. The refinement in meshless methods is easier when comparing to that of mesh based methods and it only involves insertion and deletion of required nodes. Tabarraei and Sukumar [33] presented the quadtree data structure and conforming polygonal interpolants, which are useful in developing h-adaptive finite element method. An adaptive strategy for solving nonlinear solid mechanics problems using element free Galerkin meshless method was presented by Ullah and Augarde [34]. The error estimation and adaptive strategy with natural neighbor shape functions for analysis of solid mechanics problems are available in [35, 36]. In recent years, the analysis of plate structure by meshless methods has become an emerging research area. However, there exists limited literature on error estimation and adaptive strategy in laminated plate bending analysis by meshless NEM.

In this paper, adaptive strategy is implemented in meshless natural element method for the analysis of laminated structures. The C^0 Sibson shape functions based on natural neighbor coordinates were employed in the adaptive analysis of laminated composite plates. The plate formulation is based on Reissner–Mindlin plate theory. Then the recovery based relative energy norm error estimation based on natural neighbor coordinates for a plate bending problem is presented. Initially, the present adaptive procedure was implemented to two classical elasto-static problems subjected to in-plane loads to verify the present method strategy and also,

efficacy of the method in convergence of results is studied. Then, four different cases of the laminated plates with cutouts subjected to transverse load are investigated. The location of the cutouts in the plates and the effect of boundary conditions on the cutouts are also investigated.

2 Mathematical formulation

This section presents initially the formulation of interpolation functions based on natural neighbor coordinates. Then the Reissner–Mindlin plate theory for the analysis of the laminated plates is provided. Finally, adaptive strategy is presented for the analysis of plates using present meshless method.

2.1 Natural neighbor interpolation

This section briefly describes the construction of shape functions based on natural neighbor coordinates. The interpolation is based on Voronoi cell and Delaunay tessellation. Here, 2D Euclidean space R^2 is considered. Consider a set of distinct nodes $N=\{n_1,n_2,\ldots n_{\mathrm{M}}\}$ in R^2. The first order ($k=1$) Voronoi diagram of set of nodes N in a domain is subdivision of the plane into regions T_I. Then, the Voronoi cell T_I is defined as

$$T_I = \left\{X \in R^2 : d(X,X_I) < d(X,X_J) \quad \forall J \neq I\right\}, \tag{1}$$

where $d(X, X_I)$ is the distance between points X and X_I. The construction of Voronoi cell is shown in Fig. 1.

The Delaunay triangles are constructed by connecting to natural neighbors of node I and whose Voronoi cells have common boundaries as shown in Fig. 2a. The important property of Delaunay triangles is the empty circumcircle criterion, i.e if DT(n_J, n_K, n_L) is any Delaunay triangle of nodal set N, then circumcircle of DT contains no other nodes of N. This criterion is used to find natural neighbors of a point X. The natural neighbor coordinates were introduced by Sibson [6]. Similarly, higher order ($k>1$) Voronoi cells can be constructed. Sibson used second order Voronoi cells to find natural neighbor interpolation functions. The second order Voronoi diagram of the set of nodes N in domain is a subdivision of the plane into cells T_{IJ}. The Voronoi cell T_{IJ} is defined as.

$$T_{IJ} = \left\{X \in R^2 : d(X,X_I) < d(X,X_J) < d(X,X_K) \quad \forall K \neq I,J\right\}. \tag{2}$$

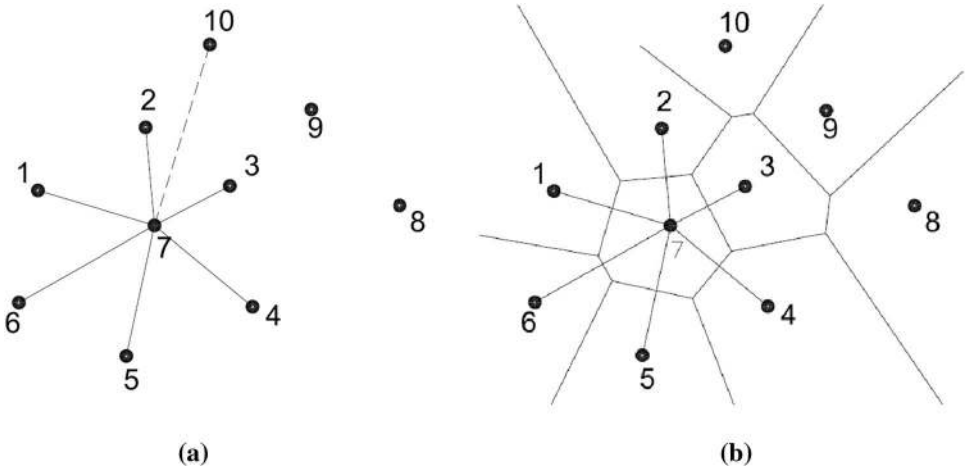

Fig. 1 Construction of Voronoi cells **a** neighbor nodes to node 7 **b** Voronoi cells with its associated nodes

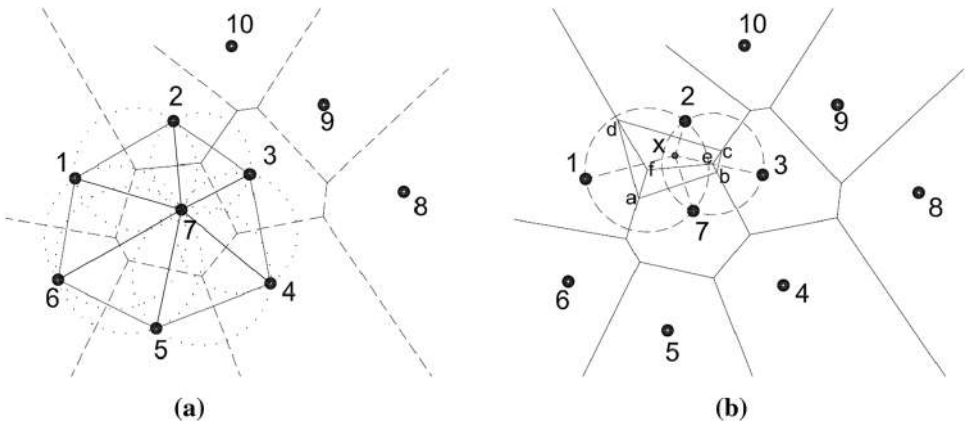

Fig. 2 Construction of second order Voronoi cell **a** Delaunay triangles ***b*** second order Voronoi cell to point X

Figure 2b shows the construction of second order Voronoi cells. Consider a point X is introduced into the Voronoi diagram of set of nodes N. Natural neighbors to the point X can be found from empty circumcircle criteria. Let the X lies within the circumcircle of a triangle DT(n_J, n_K, n_L), then n_J, n_K, and n_L are its natural neighbors.

The bisectors to the lines connecting to the point X to its natural neighbors form second order Voronoi cell T_X (closed polygon *abcd*). Here, the X has four natural neighbors ($n=4$) namely 1, 2, 3 and 7. The natural neighbor coordinates of point X with respect to natural neighbor I is defined as

$$\phi_I(X) = \frac{A_I(X)}{A(X)}, \tag{3}$$

where I ranges from 1 to n and $A(X) = \sum_{J=1}^{n} A_J(X)$. For example, the shape function for the node 2 is written as $\phi_2(X) = A_{dcfe} \big/ A_{abcd}$. For more details about shape functions refer Sukumaret al. [7]. The properties of the shape function are

$$\text{Interpolation property } \begin{matrix} 0 \leqslant \phi_I(X) \leqslant 1 \\ \phi_I(X_J) = \delta_{IJ} \end{matrix}, \tag{4}$$

$$\text{Partition of unity } \sum_{I=1}^{n} \phi_I(X) = 1, \tag{5}$$

$$\text{Linear completeness } X = \sum_{I=1}^{n} \phi_I(X) X_I. \tag{6}$$

The displacement field $u(X)$ at a point X is expressed in terms of shape functions and unknown displacements u_I as

$$u(X) = \sum_{I=1}^{n} \phi_I(X) u_I, \tag{7}$$

where u_I ($I=1,2,\ldots n$) are vectors of nodal displacements at n natural neighbors and $\phi_I(X)$ are the shape functions associated with each node. The shape function of central node of the domain is shown in Fig. 3b.

2.2 2D plate theory formulation

The displacement filed of Reissner–Mindlin plate theory is written as

$$\begin{aligned} u(x,y,z) &= u_0(x,y) + z\theta_x(x,y) \\ v(x,y,z) &= v_0(x,y) + z\theta_y(x,y) \\ w(x,y,z) &= w_0(x,y), \end{aligned} \tag{8}$$

where u_0, v_0 and w_0 are displacements of a point on the plane $z=0$. θ_x and θ_y are rotations of a transverse normal about y- and x-axis, respectively. In Reissner–Mindlin plate theory, the displacement field is expressed till first order of z term, so it is also known as first order shear deformation plate theory (FSDT).

The in-plane strain–displacement relation can be given as

$$\begin{Bmatrix} \varepsilon_{xx} \\ \varepsilon_{yy} \\ \gamma_{xy} \end{Bmatrix} = \begin{Bmatrix} \frac{\partial u}{\partial x} \\ \frac{\partial v}{\partial y} \\ \frac{\partial u}{\partial y} + \frac{\partial v}{\partial x} \end{Bmatrix} = \begin{Bmatrix} \varepsilon_{xx}^{(0)} \\ \varepsilon_{yy}^{(0)} \\ \gamma_{xy}^{(0)} \end{Bmatrix} + z \begin{Bmatrix} k_{xx}^{(1)} \\ k_{yy}^{(1)} \\ k_{xy}^{(1)} \end{Bmatrix}. \tag{9}$$

Transverse shear strains

$$\begin{Bmatrix} \gamma_{xz} \\ \gamma_{yz} \end{Bmatrix} = \begin{Bmatrix} \frac{\partial u}{\partial z} + \frac{\partial w}{\partial x} \\ \frac{\partial v}{\partial z} + \frac{\partial w}{\partial y} \end{Bmatrix} = \begin{Bmatrix} \gamma_{xz}^{(0)} \\ \gamma_{yz}^{(0)} \end{Bmatrix}, \tag{10}$$

where

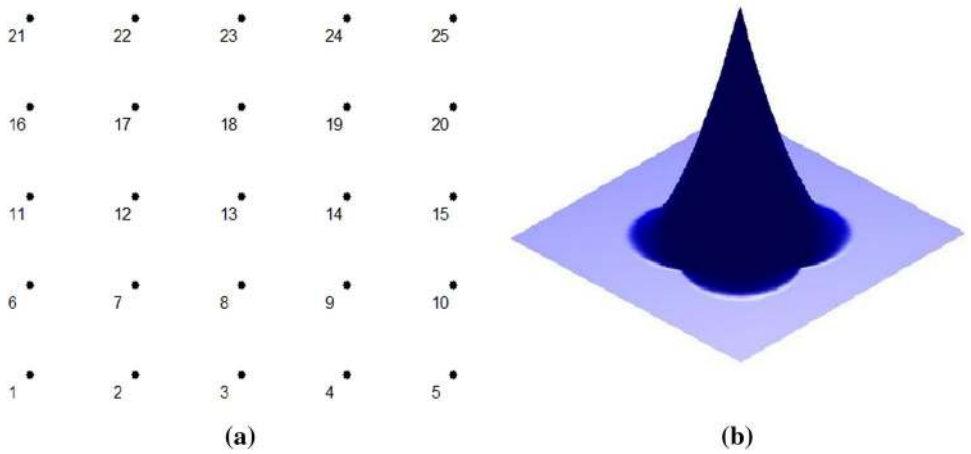

Fig. 3 Shape function in a given domain **a** equispaced nodes in the domain **b** C^0 shape function to the central node 13

$$\begin{Bmatrix} \varepsilon_{xx}^{(0)} \\ \varepsilon_{yy}^{(0)} \\ \gamma_{xy}^{(0)} \end{Bmatrix} = \begin{Bmatrix} \frac{\partial u_0}{\partial x} \\ \frac{\partial v_0}{\partial y} \\ \frac{\partial u_0}{\partial y} + \frac{\partial v_0}{\partial x} \end{Bmatrix} \begin{Bmatrix} k_{xx}^{(1)} \\ k_{yy}^{(1)} \\ k_{xy}^{(1)} \end{Bmatrix} = \begin{Bmatrix} \frac{\partial \theta_x}{\partial x} \\ \frac{\partial \theta_y}{\partial y} \\ \frac{\partial \theta_x}{\partial y} + \frac{\partial \theta_y}{\partial x} \end{Bmatrix} \begin{Bmatrix} \gamma_{xz}^{(0)} \\ \gamma_{yz}^{(0)} \end{Bmatrix} = \begin{Bmatrix} \theta_x + \frac{\partial w_0}{\partial x} \\ \theta_y + \frac{\partial w_0}{\partial y} \end{Bmatrix}. \tag{11}$$

Constitutive relation of the laminate is written in lamina coordinate (*x, y, z*) system. The in-plane stress strain relation for the *k*th lamina can be givens as

$$\begin{Bmatrix} \sigma_x \\ \sigma_y \\ \tau_{xy} \end{Bmatrix} = \begin{bmatrix} Q_{11} & Q_{12} & Q_{16} \\ Q_{12} & Q_{22} & Q_{26} \\ Q_{16} & Q_{26} & Q_{66} \end{bmatrix} \begin{Bmatrix} \varepsilon_x \\ \varepsilon_y \\ \gamma_{xy} \end{Bmatrix}, \tag{12}$$

$$\{\sigma\} = [Q]\{\varepsilon\} \tag{13}$$

Shear stress strain relation

$$\begin{Bmatrix} \tau_{yz} \\ \tau_{xz} \end{Bmatrix} = \begin{bmatrix} Q_{55} & Q_{54} \\ Q_{54} & Q_{44} \end{bmatrix} \begin{Bmatrix} \gamma_{yz} \\ \gamma_{xz} \end{Bmatrix}, \tag{14}$$

$$\{\tau\} = \left[Q^s\right]\{\gamma\}, \tag{15}$$

where $[Q_{ij}]$ are transformed material constants. The elements of $[Q_{ij}]$ are given as

$$[Q_{ij}] = [T_1]^{-1}[C_{ij}]_k[T_1]^{-\mathrm{T}} \quad (i,j = 1,2,6), \tag{16}$$

$$[Q_{ij}] = [T_2]^{-1}[C_{ij}]_k[T_2]^{-\mathrm{T}} \quad (i,j = 5,4), \tag{17}$$

where $[T_1]$ and $[T_2]$ are the transformation matrices. $[C_{ij}]_k$ is the constitutive matrix at the k^{th} lamina level.

$$\left[T_1\right] = \begin{bmatrix} \mathrm{c}^2 & s^2 & 2cs \\ s^2 & \mathrm{c}^2 & -2cs \\ -cs & cs & \mathrm{c}^2 - s^2 \end{bmatrix}, \tag{18}$$

$$\left[T_2\right] = \begin{bmatrix} c & s \\ -s & c \end{bmatrix}, \tag{19}$$

c—cosθ, s—sinθ and θ—orientation of fiber in anti-clockwise direction to *x*-axis

$$\left[C_{ij}\right]_k = \begin{bmatrix} C_{11} & C_{12} & 0 \\ C_{12} & C_{22} & 0 \\ 0 & 0 & C_{66} \end{bmatrix} \quad (i,j = 1,2,6), \tag{20}$$

$$\left[C_{ij}\right]_k = \begin{bmatrix} C_{55} & 0 \\ 0 & C_{44} \end{bmatrix} \quad (i,j = 5,4), \tag{21}$$

where $C_{11} = E_1/(1 - \nu_{12}\nu_{21})$, $C_{12} = \nu_{12}E_2/(1 - \nu_{12}\nu_{21})$, $C_{22} = E_2/(1 - \nu_{12}\nu_{21})$, $C_{66} = G_{12}$, $C_{55} = G_{13}$, $C_{44} = G_{23}$ material properties with respect to fiber matrix coordinate axes (1, 2, 3).

The equations of equilibrium for the stress analysis are obtained using principle of minimum potential energy. In analytical form it can be written as

$$\delta(U + W) = 0, \tag{22}$$

where U is total strain energy due to deformation, W is the potential of external loads, and $U + W = I$ is the total potential energy.

$$\text{For minimum potential energy,} \quad \delta I = 0, \tag{23}$$

$$\delta I = \int_{-h/2}^{h/2} \int_A \left(\sigma_x \delta\varepsilon_x + \sigma_y \delta\varepsilon_y + \sigma_z \delta\varepsilon_z + \tau_{xy}\delta\gamma_{xy} + \tau_{yz}\delta\gamma_{yz} + \tau_{xz}\delta\gamma_{xz}\right)\mathrm{d}A\,dz - \int_A (q\delta w)\mathrm{d}A = 0. \tag{24}$$

The independent variables are $u_0, v_0, w_0, \theta_x, \theta_y$and for more details refer Reddy [8].

Boundary conditions obtained from governing equations and are given as;

Simply supported boundary conditions are $u_{0,}v_{0,}\theta_{x,} = 0$ for $x = 0$ to a and $u_{0,}v_{0,}\theta_{y,} = 0$ for $y = 0$ to b. Then for clamped all edges boundary conditions are $u_{0,}v_{0,}\theta_{x,}\theta_y = 0$ for $x = 0$ to a, and $y = 0$ to b.

Galerkin formulation

$\{\delta_i\}$—degrees of freedom at each node

$$\left\{\delta_i\right\} = \left\{ u_0 \;\; v_0 \;\; w_0 \;\; \theta_x \;\; \theta_y \right\}^{\mathrm{T}}, \tag{25}$$

where $i = 1,2\ldots,N$, N—no. of nodes

$$u_0(X) = \sum_{I=1}^{n} \phi_I(X) u_{0I}, \tag{26}$$

$$v_0(X) = \sum_{I=1}^{n} \phi_I(X) v_{0I}, \tag{27}$$

$$w_0(X) = \sum_{I=1}^{n} \phi_I(X) w_{0I}, \tag{28}$$

$$\theta_x(X) = \sum_{I=1}^{n} \phi_I(X) \theta_{xI}, \tag{29}$$

$$\theta_y(X) = \sum_{I=1}^{n} \phi_I(X) \theta_{yI}. \tag{30}$$

For static loads, the total potential energy is $(I) = U + W$

$$I = \frac{1}{2} \int_V \left(\sigma_x \varepsilon_x + \sigma_y \varepsilon_y + \tau_{xy}\gamma_{xy} + \tau_{yz}\gamma_{yz} + \tau_{xz}\gamma_{xz}\right) \mathrm{d}V - \int_A (q\, w) \mathrm{d}A. \tag{31}$$

Strain energy part (U) in above equation is written as

$$U = \frac{1}{2} \int_V \left\{ \sigma_x \;\; \sigma_y \;\; \tau_{xy} \right\} \begin{Bmatrix} \varepsilon_x \\ \varepsilon_y \\ \gamma_{xy} \end{Bmatrix} \mathrm{d}V + \frac{1}{2} \int_V \left\{ \tau_{xz} \;\; \tau_{yz} \right\} \begin{Bmatrix} \gamma_{xz} \\ \gamma_{yz} \end{Bmatrix} \mathrm{d}V = \frac{1}{2} \int_V \{\sigma\}^{\mathrm{T}} \{\varepsilon\} \mathrm{d}V + \frac{1}{2} \int_V \{\tau\}^{\mathrm{T}} \{\gamma\} \mathrm{d}V, \tag{32}$$

$$U = \frac{1}{2} \int_V \{\varepsilon\}^{\mathrm{T}} [Q] \{\varepsilon\} \mathrm{d}V + \frac{1}{2} \int_V \{\gamma\}^{\mathrm{T}} \left[Q_s\right] \{\gamma\} \mathrm{d}V, \tag{33}$$

$$U = \frac{1}{2} \int_h \int_A \{\varepsilon\}^{T} [Q] \{\varepsilon\} dA\, dh + \frac{1}{2} \int_h \int_V \{\gamma\}^{T} \left[Q_s\right] \{\gamma\} dA\, dh \tag{34}$$

$$\left(A_{ij}, B_{ij}, D_{ij}\right) = \int_{h_L}^{h_{L+1}} Q_{ij}(1, z, z^2) \mathrm{d}z \quad \text{where } i,j = 1,2,6, \tag{35}$$

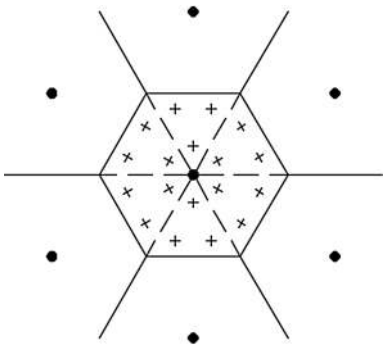

Fig. 5 Integration points '+' in triangles of Voronoi cell

$$A_{ij}^{s} = \int_{h_L}^{h_{L+1}} Q_{ij}^{s} \mathrm{d}z \quad \text{where } i,j = 5,4. \tag{36}$$

The total potential energy (I) can be written as

$$= \frac{1}{2} \int_A \left(\left\{\varepsilon^{(0)}\right\}^{\mathrm{T}} [A] \left\{\varepsilon^{(0)}\right\} + \left\{k^{(1)}\right\}^{\mathrm{T}} [B] \left\{\varepsilon^{(0)}\right\} + \left\{\varepsilon^{(0)}\right\}^{\mathrm{T}} [B] \left\{k^{(1)}\right\} + \left\{k^{(1)}\right\}^{\mathrm{T}} [D] \left\{k^{(1)}\right\} + \frac{1}{2} \int_A \left(\left\{\gamma^{(0)}\right\}^{T} \left[A^s\right] \left\{\gamma^{(0)}\right\} \right) \mathrm{d}A - \int_A qw \mathrm{d}A \right. \tag{37}$$

for minimum total potential energy $\delta I = 0$, then we get

$$[K]\{\delta\} = \{F\}. \tag{38}$$

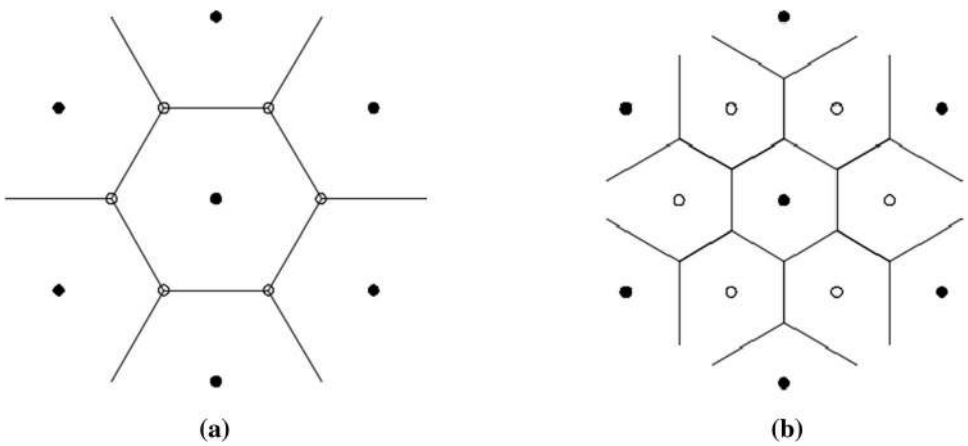

Fig. 4 Nodal refinement strategy, '**o**' are new nodes introduced at vertices of Voronoi cell. **a** Initial Voronoi cell and **b** Voronoi cells after refinement

2.3 Error estimation and adaptive procedure

The recovery stress is used as an error estimator and then relative energy norm of the error (η_i) is basis for refinement. The energy norm of the error is calculated for each Voronoi cell, then the maximum error of the Voronoi cells is not met the refinement criteria, then the particular cell will be refined by introducing new nodes. The introduction of new nodes at vertices of Voronoi cell and nodal refinement strategy is explained in Fig. 4. The discretization error σ^{e}in stress field at any point given as the difference between the stresses returned at Gauss (integration) points inside triangles of Voronoi cells and the recovered stress field is calculated from stresses at Gauss points but using interpolation function based on natural neighbors coordinates. Calculation of stresses inside Voronoi cell is done as shown in Fig. 5. A similar approach adopted for error estimation based on natural neighbor coordinates in Yvonnet et al. [36].

$$\sigma^{\mathrm{e}} = \hat{\sigma}(X) - \sigma(X) \quad \tau^{\mathrm{e}} = \hat{\tau}(X) - \tau(X). \tag{39}$$

The stress vector at any point X is written as

$$\sigma(X) = [Q]\{\varepsilon\} \quad \tau(X) = [Q_s]\{\tau\}. \tag{40}$$

The recovery stress field at any point X is written as

$$\hat{\sigma}(X) = \sum_{i=1}^{n} \phi_i(X)\sigma(X_i) \quad \hat{\tau}(X) = \sum_{i=1}^{n} \phi_i(X)\tau(X_i), \tag{41}$$

where $\phi_i(X)$ is the natural neighbor interpolation functions at a point X, n is number of natural neighbor nodes to point X. Error for the individual Voronoi cell and for the whole domain can be calculated using appropriate norm. In a particular Voronoi cell, the error in energy norm is written as

$$\|e\| = \left\| U^{\hat{\sigma}} - U^{\sigma} \right\|_{\Omega_i}. \tag{42}$$

The recovery strain energy norm $U^{\hat{\sigma}}$ for the domain is written as

$$\left\| U^{\hat{\sigma}} \right\| = \left[\int_{\Omega} \left| (\hat{\sigma}(X))^T Q^{-1} \hat{\sigma}(X) + (\hat{\tau}(X))^T Q_s^{-1} \hat{\tau}(X) \right| \mathrm{d}\Omega \right]^{\frac{1}{2}}. \tag{43}$$

The integrals of the Eqs. (42) and (43) are evaluated at Gauss points inside the triangles of the Voronoi cells. The relative energy norm is an error estimator for adaptive analysis and is written as

$$\eta_i = \frac{\|e\|_{\Omega_i}}{\left\| U^{\hat{\sigma}} \right\|_{\Omega}} \times 100. \tag{44}$$

Adaptive procedure

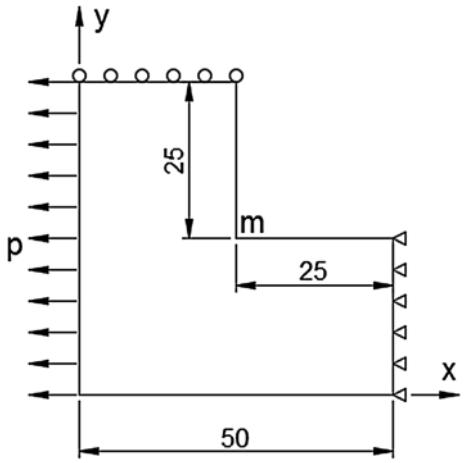

Fig. 6 Load and boundary conditions of L plate

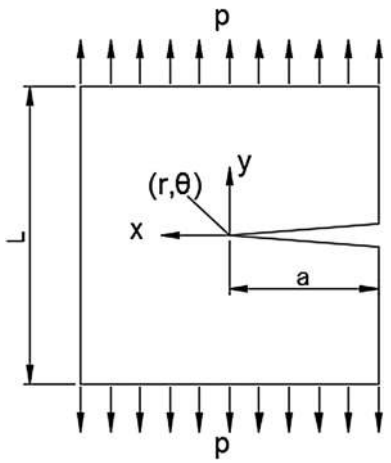

Fig. 7 Square plate ($L = 100$) with crack size ($a = 50$)

1. Start of analysis, define problem and apply load and boundary conditions.
2. Solve Eq. (38) for the displacements at nodes in the domain.
3. Calculate strains and stresses at Gauss points inside the triangles of the Voronoi cells.
4. Calculate recovery strains and stresses from stresses of above step but based on natural neighbor interpolation.
5. Calculate energy error norm in each cell and strain energy of the whole domain.
6. Find relative energy norm of each Voronoi cell using Eq. (44).
7. Check the refinement criterion for each cell, if satisfied exit analysis.
8. Otherwise, introduce new nodes at the vertices of the Voronoi cell, where the criterion is not met. Then, repeat

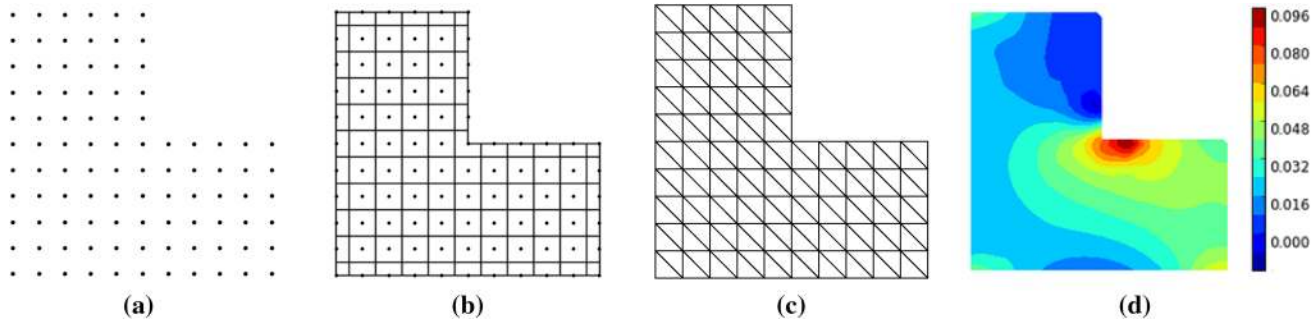

Fig. 8 *L* plate before adaptivity, **a** nodes, **b** Voronoi cells, **c** background mesh, **d** stress σ_{xx} in the plate

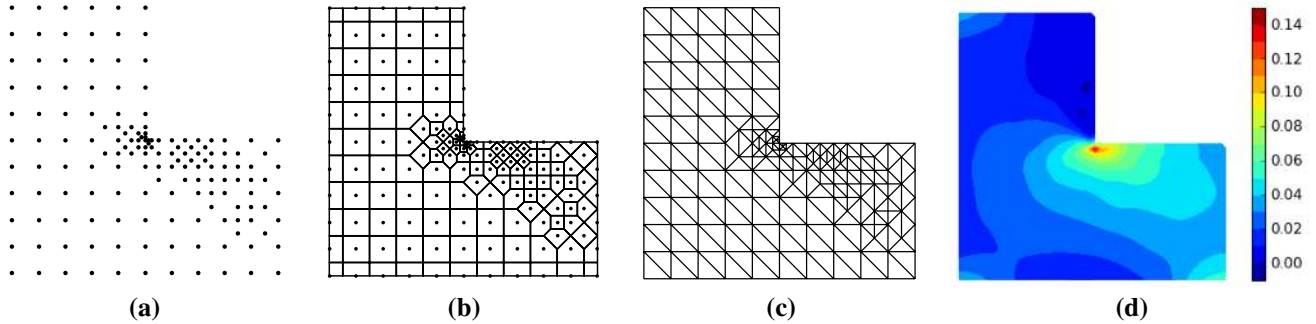

Fig. 9 *L* plate in final iteration of adaptivity, **a** nodes, **b** Voronoi cells, **c** background mesh, **d** stress σ_{xx} in the plate

the same procedure until the refinement criterion is satisfied.

3 Numerical problems

Initially, adaptive procedure of the present method is applied to two elastostatic classical problems. These are plane stress problems subjected to only in-plane loads and transverse shear stresses are ignored. Then the composite laminate plates with cutouts subjected to transverse loads are investigated. Matlab program is written based on present method for the analysis problems. Firstly, consider in-plane problem where *L* plate subjected to unit traction *P* in horizontal direction and boundary conditions are applied as shown in Fig. 6. Then the other in-plane load problem is the plate with mode *I* crack with crack size *a* subjected to unit traction in vertical direction as shown in Fig. 7. This problem has analytical solution for calculating stresses at crack tip. An isotropic material is considered for above two problems with unit thickness and material properties are modulus of elasticity $E=3\times10^7$ and Poisson's ratio $v=0.3$. Stresses at a node are calculated by averaging stresses at Gauss points near to the node and stress plots for different cases have been extracted from the analysis. The refinement criterion is 0.3%

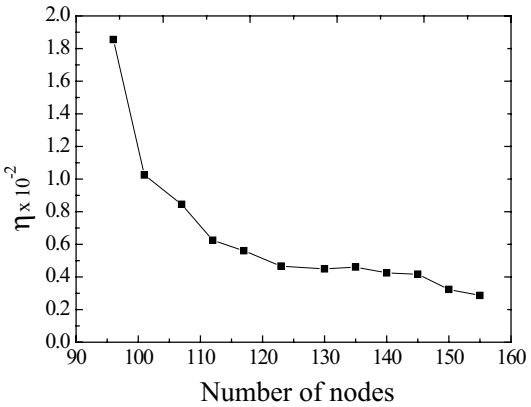

Fig. 10 Rate of convergence, nodes versus relative energy norm of the error

for all problems in this paper, if any of the Voronoi cell did not meet the criterion, the adaptive procedure repeats till the criterion is met.

Let us consider *L* plate, which is subjected to unit traction *P* and constraints as shown in Fig. 6. The plate will have stress singularity at corner point *m* for applied loads and refinement is expected to take place at that corner area. Initial nodal density in the plate is shown in Fig. 8a. and

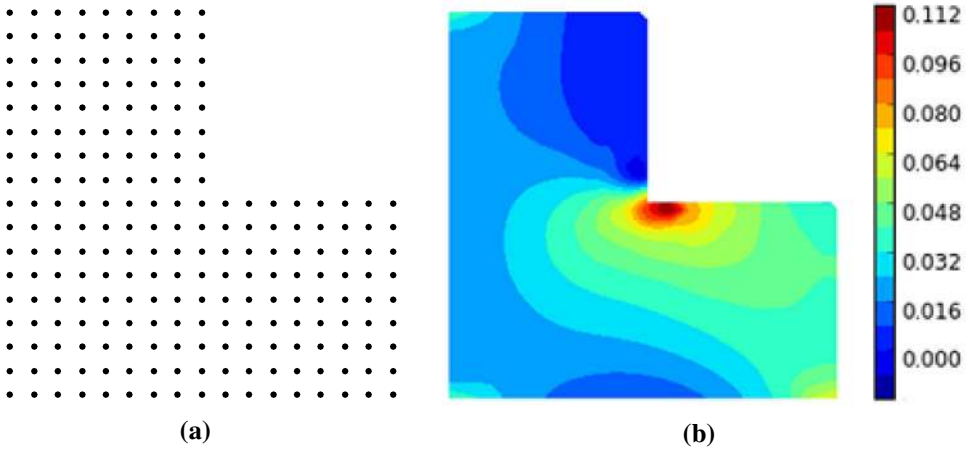

Fig. 11 *L* plate with no adaptivity, **a** nodes, 225, **b** stress σ_{xx} in the plate

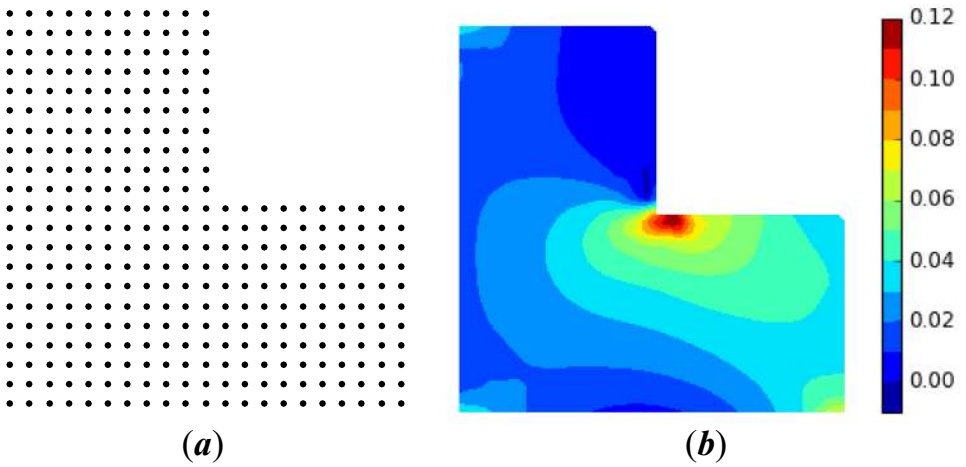

Fig. 12 *L* plate with no adaptivity, **a** nodes, 341, **b** stress σ_{xx} in the plate

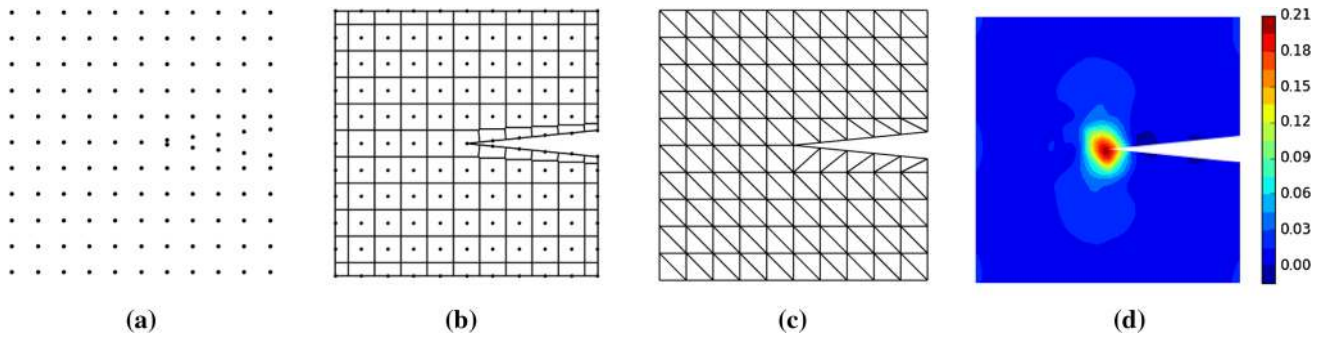

Fig. 13 A square plate with crack before adaptivity, **a** nodes, **b** Voronoi cells, **c** background mesh, **d** stress σ_{yy} in the plate

respective background triangles for integration and Voronoi cells are shown in Fig. 8b, c, respectively. Initial nodal density in the domain is 96 and the maximum percentage of error is 1.85 at the corner point *m* in the plate. Also, stress (σ_{xx}) is maximum at same point and its value is 0.096 units, as shown in Fig. 8d. Then, adaptivity in the plate is carried until the error criterion is met and during each iteration the percentage of error of each cell is calculated to check the criterion. The final nodal density of the plate is 155 and is shown in Fig. 9a. For this case, the highest percentage of error in the domain is 0.28% and it is lower than defined criterion 0.3% for refinement. The maximum stress in the final iteration is 0.14 at the point *m* in the plate, as shown in Fig. 9d. The rate of convergence of solution, nodes versus

percent of error, is shown in Fig. 10. The convergence rate is higher for initial five iterations and then it is very gradual till the final iteration. The same problem is investigated without adaptivity to assess the computational efficiency and accuracy of the results. Consider the L plate with uniformly distributed nodes 225 and 341, as shown in Figs. 11a and 12a, respectively. The maximum percentage of error for these cases is 1.07 and 0.80, respectively. The maximum stresses obtained with no adaptivity are lower than that of the stresses obtained with adaptivity analysis. Also, decrease in percentage of error is not in same proportion with increase in nodal density from 225 to 341. Therefore, the convergence rate is not higher with no adaptivity cases when comparing to adaptivity analysis.

Now consider a square plate with mode-I crack and is subjected to load as shown in Fig. 7. The tip of crack in the plate will subject to stress singularity for the applied load and the refinement is expected to happen at the tip of the crack. Initial nodal density in the plate is 126, shown in Fig. 13a and corresponding Voronoi cells and Delaunay triangles are shown in Fig. 13b, c, respectively. The maximum error is 27.96% at the tips of the crack and stress (σ_{yy}) field at the tip of crack is shown in Fig. 13d. The analytical solution [42] for stress field of this problem can be written as.

$$\begin{aligned}
\sigma_{xx} &= \frac{K_I}{\sqrt{2\Pi r}} \cos\frac{\theta}{2}\left(1 - \sin\frac{\theta}{2}\sin\frac{3\theta}{2}\right),\\
\sigma_{yy} &= \frac{K_I}{\sqrt{2\Pi r}} \cos\frac{\theta}{2}\left(1 + \sin\frac{\theta}{2}\sin\frac{3\theta}{2}\right),\\
\sigma_{xy} &= \frac{K_I}{\sqrt{2\Pi r}} \sin\frac{\theta}{2}\cos\frac{\theta}{2}\cos\frac{3\theta}{2} \quad \text{where } K_I = p\sqrt{\Pi a}.
\end{aligned} \tag{45}$$

The refinement never ends for this problem due to stress singularity at the tip of the crack, so computation is terminated when the error criterion 0.40% is satisfied. The criterion is met in eighth iteration and the corresponding nodal density (177), Voronoi cells and background cell are shown in Fig. 14a–c, respectively. The stress (σ_{yy}) for this case is 0.48 and its distributions at the crack tip shown in Fig. 14d. The stress is more precisely located at very near tip of the

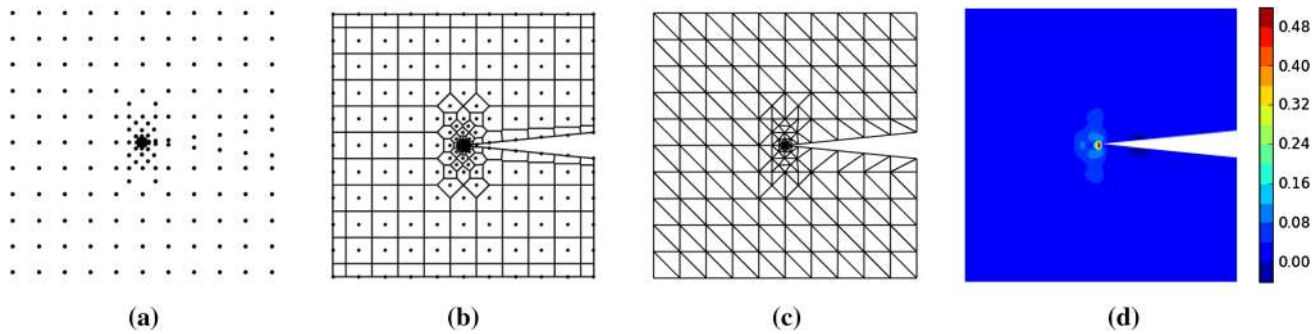

Fig. 14 A square plate with crack after adaptivity, **a** nodes, **b** Voronoi cells, **c** background mesh, **d** stress σ_{yy} in the plate

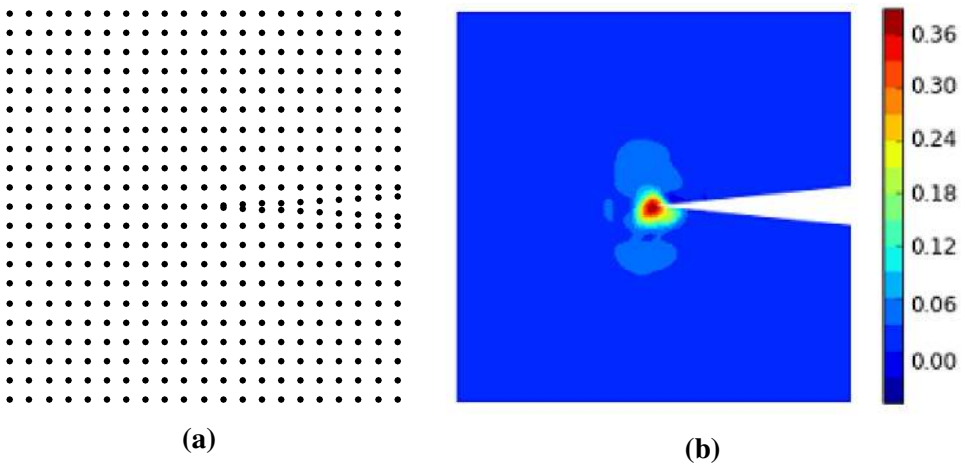

Fig. 15 Plate with crack, **a** nodes, 451, **b** stress σ_{yy} in the plate

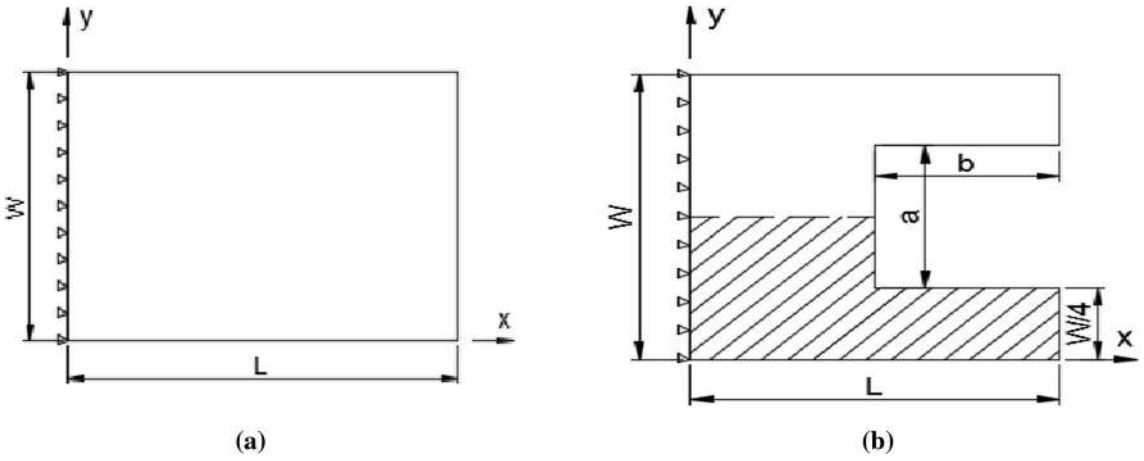

Fig. 16 Rectangular ($L=2W=100$) cantilever composite plate subjected to transverse load ($q=0.2$/unit length) at free edge, **a** no cutout, **b** with slot at free end ($a=W/2$, $b=L/2$)

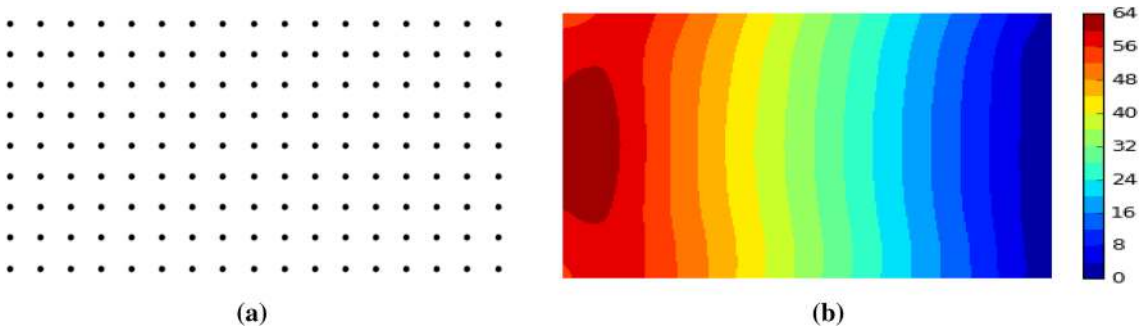

Fig. 17 Cantilever plate subjected transverse load at free end, **a** nodes (153), **b** stress, σ_{xx}

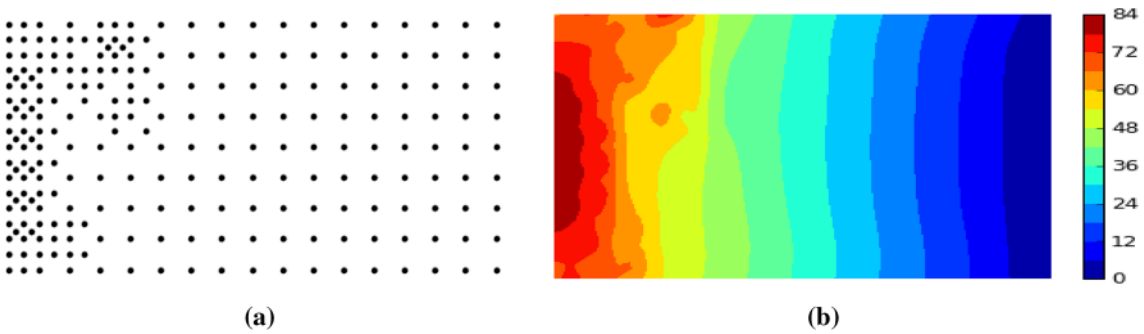

Fig. 18 Cantilever plate subjected transverse load at free end, **a** nodes (236), **b** stress, σ_{xx}

crack and not distributed widely when compare with stress field obtained in the iteration one. The stress (σ_{yy}) obtained using present method is in good agreement with analytical solution at near the crack tip. Further, this problem also analyzed with higher number of nodes, but is uniformly distributed in the plate, as shown in Fig. 15a. The percentage of error in this case is 20 and the stress filed in the plate is shown in Fig. 15b.

Numerical problems on composite plates In this section symmetric lamina lay-up (0°/90°/0°) composite plates subjected to transverse load are investigated. The material properties of the lamina are $E_1=25$, $E_2=1$, $G_{12}=G_{13}=0.5E_2$, $G_{23}=0.2E_2$, $v_{12}=v_{13}=0.25$. Thickness of the laminate plate

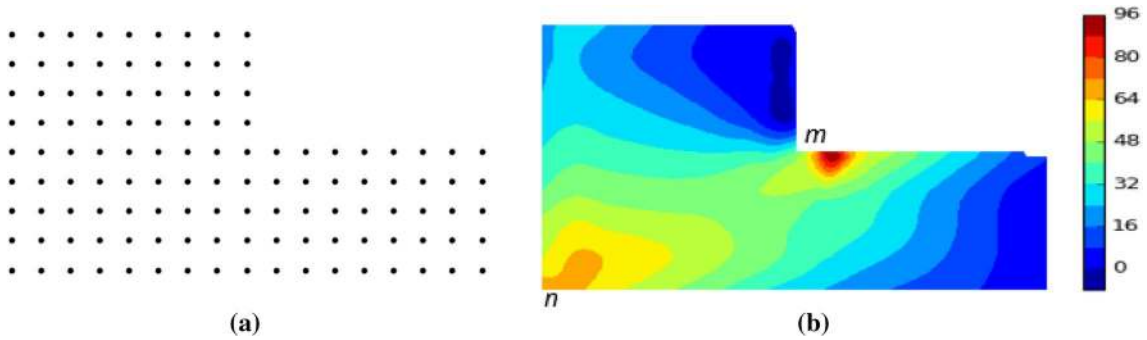

Fig. 19 Cantilever plate with cutout subjected to transverse load, **a** nodes (121), **b** stress, σ_{xx}

is 1 unit and all laminae of the plate are of equal thickness. Initially, laminated plate subjected to cantilever load is analyzed, then the laminate with cutout is investigated with present adaptive procedure. Analysis of cantilever plates without cutout and with slot at free end subject transverse load is carried-out, shown in Fig. 16a, b, respectively. Influence of location of the cutouts in the plate and boundary conditions of the plate are investigated.

In this section, laminated composite rectangular cantilever plates subjected to transverse loads at free end are investigated. Consider the cantilever plate for the adaptivity analysis as shown in Fig. 16a. It is obvious from the plate geometry, load and boundary conditions that the plate will have maximum stress at the fixed end. Initially, the analysis of plate with uniformly distributed nodes is carried-out. The maximum relative energy norm of error is 0.37% with the initial node count over the domain 153. The maximum stress at fixed end of the plate is 64 units and can be seen in Fig. 17b. Then the plate analysis is continued with adaptive strategy until the error criterion, 0.25%, is met. The node count in the final iteration is 236 and the maximum stress at fixed end is 84 units, shown in Fig. 18a, b, respectively. The stress obtained in the final iteration is around 30% higher when compare to that of initial iteration. That means the accuracy of the results is improved with adaptivity and also location of the stress field is more precisely located near the fixed edge of the plate as seen in Fig. 18b.

Consider the laminate plate with end slot subjected to transverse load at free edge of the plate as shown in Fig. 16b. The geometry of the plate is symmetrical at the center about horizontal axis, so half geometry of the plate is modeled for the reason of less computational effort. The plate is analyzed with initial nodal density 121, as shown in Fig. 19a. The percentage of error with initial nodal density is 0.61 and the maximum stress in the plate is 96 units at corner area (*m*) of the cut section. It can be seen in Fig. 19b that the plate also has higher stress at fixed edge near point *n* of the plate. It can be estimated from stress contour plot that the weakest section of the geometry for the applied loads would be straight line connection point *m* and *n*. It is because of presence of higher stresses along the section. Further, the plate is analyzed with adaptive procedure until the error criterion 0.20% is met. The nodal density (259) over the domain in the final iteration of the adaptive analysis is shown in Fig. 20a. The stress contour plot for the final iteration is shown in Fig. 20b. The maximum stress is occurring near point *m* and *n* and is around 112 units. Furthermore, the maximum stress locations and magnitude of this case are different when compare to the same plate with no slot (previous case). Also, it can be seen in Fig. 20a that the more nodes are introduced in

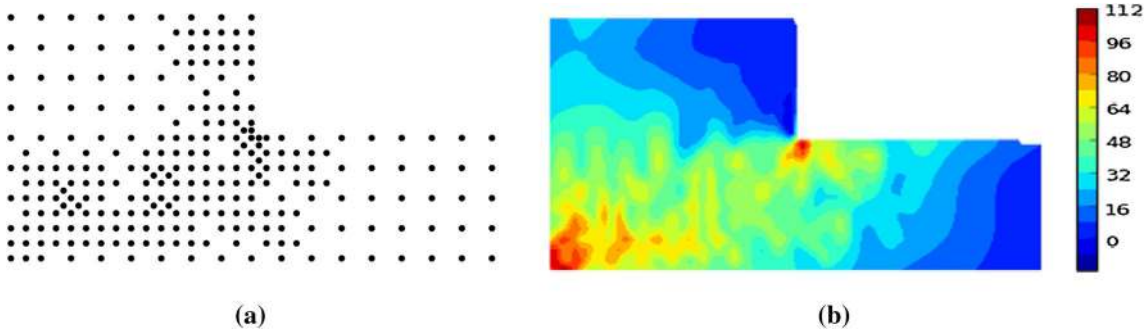

Fig. 20 Cantilever plate with cutout subjected to transverse load, **a** nodes (259), **b** stress, σ_{xx}

the weakest area of the geometry. It can be concluded that the results of adaptive analysis also useful in revealing the failure prone areas of the plate with cutouts subjected to different loads.

4 Conclusion

Meshless method based on natural neighbor coordinates for the adaptive analysis of plates and laminated composite plates is presented. The error estimation for adaptive strategy is based on stress recovery. Then the analysis of the plates and laminates subjected to in-plane and transverse loads is carried-out using first shear deformation plate theory. Then the efficacy of the present method is assessed with classical problems. It is observed that the present adaptive procedure provides accurate results with lower computational cost when compare to the results of no adaptivity. Then influence of boundary conditions on laminated composite plates with cutouts subjected to transverse loads is investigated. The adaptivity in the plates is taken place at stress singularities areas. The refined area in the domain indicates the area under higher stresses and it means these are failure prone areas of the geometry for given load conditions. Cantilever plates with and without slot subjected to transverse loads at free end have different maximum stress values and also their locations are not same. It can be said that the adaptive strategy in the plate analysis using meshless method provides accurate results at lower computational effort.

References

1. Belytschko T, Lu YY, Gu Y (1994) Element free Galerkin method. Int J Numer Methods Eng 37:229–256. https://doi.org/10.1002/nme.1620370205
2. Atluri SN, Zhu T (1998) A new meshless local Petrov–Galerkin approach in computational mechanics. Comput Mech 22(2):117–127. https://doi.org/10.1007/s004660050346
3. Monaghan JJ (1977) Smoothed particle hydrodynamics: theory and applications to non-spherical stars. Mon Not R Astron Soc 181:375–389. https://doi.org/10.1093/mnras/181.3.375
4. Bathe KJ, De S (2001) Towards an efficient meshless computational technique: the method of finite spheres. Eng Comput 18:170–192. https://doi.org/10.1108/02644400110365860
5. Sambridge MS, Braun J, McQueen H (1995) Geophysical parametrization and interpolation of irregular data using natural neighbours. Geophys J Int 122(1):837–857. https://doi.org/10.1111/j.1365-246X.1995.tb06841.x
6. Sibson R (1980) A vector identity for the Dirichlet tessellation. Math Proc Camb Philos Soc 87:151–155. https://doi.org/10.1017/S0305004100056589
7. Sukumar N, Moran B, Belytschko T (1998) The natural element method in solid mechanics. Int J Numer Methods Eng 43(5):839–887. http://doi.org/10.1002/(SICI)1097-0207(19981115)43:5<839::AID-NME423>3.0.CO;2-R
8. Reddy JN (2004) Mechanics of laminated composite plates and shells theory and analysis, 2nd edn. CRC Press, Boca Raton
9. Chate A, Makinen K (1994) Plane finite element for static and free vibration analysis of sandwich plates. Mech Compos Mater 30(2):168–176. https://doi.org/10.1007/BF00635849
10. Lee LJ, Fan YJ (1996) Bending and vibration analysis of composite sandwich plates. Comput Struct 60(1):103–112. https://doi.org/10.1016/0045-7949(95)00357-6
11. Reddy JN, Cho WC (1981) Non-linear bending of thick rectangular, laminated composite plates. Int J Non Linear Mech 16(3&4), 291–301. https://doi.org/10.1016/0020-7462(81)90042-1
12. Wung PM, Reddy JN (1991) A transverse deformation theory of laminated composite plates. Comput Struct 41(4):821–833. https://doi.org/10.1016/0045-7949(91)90191-N
13. Reddy JN (1984) A simple higher order theory for laminated composite plates. J Appl Mech T ASME 51:745–752. https://doi.org/10.1115/1.3167719
14. Reddy JN, Phan ND (1985) Stability and vibration of isotropic, orthotropic and laminated plates according to a higher order shear deformation theory. J Sound Vib 98(2):157–170. https://doi.org/10.1016/0022-460X(85)90383-9
15. Lim SP, Lee KH, Chow ST, Senthilnathan NR (1988) Linear and non-linear bending of shear deformable plates. Comput Struct 30(4):945–952. https://doi.org/10.1016/0045-7949(88)90132-0
16. Madhukar S, Singha MK (2013) Geometrically nonlinear finite element analysis of sandwich plates using normal deformation theory. Compos Struct 97:84–90. https://doi.org/10.1016/j.compstruct.2012.10.034
17. Nayak AK, Moy SSJ, Shenoi RA (2002) Free vibration analysis of composite sandwich based on Reddy's higher order theory. Compos Part B Eng 33:505–519. https://doi.org/10.1016/S1359-8368(02)00035-5
18. Pandya BN, Kant T (1988) A refined higher order generally orthotropic C_0 plate bending element. Comput Struct 28(2):119–133. https://doi.org/10.1016/0045-7949(88)90031-4
19. Dinis LMJS., Jorge RMN, Belinha J (2007) Analysis of 3D solids using the natural neighbor radial point interpolation method. Comput Methods Appl Mech Eng 196:2009–2028. https://doi.org/10.1016/j.cma.2006.11.002
20. Dinis LMJS., Jorge RMN, Belinha J (2008) Analysis of plates and laminates using the natural neighbor radial point interpolation method. Eng Anal Bound Elem 32:267–279. https://doi.org/10.1016/j.enganabound.2007.08.006
21. Dinis LMJS., Jorge RMN, Belinha J (2010) A 3D shell-like approach using a natural neighbor meshless method: isotropic and orthotropic thin structures. Compos Struct 92:1132–1142. https://doi.org/10.1016/j.compstruct.2009.10.014
22. Dinis LMJS., Jorge RMN, Belinha J (2011) A natural neighbor meshless method with a 3D shell-like approach in the dynamic analysis of thin 3D structures. Thin Wall Struct 49:185–196. https://doi.org/10.1016/j.tws.2010.09.023
23. Leung AYT (1991) An unconstrained third order plate theory. Comput Struct 40(4):871–875. https://doi.org/10.1016/S0045-7949(03)00290-6
24. Dinis LMJS., Jorge RMN, Belinha J (2010) An unconstrained third order plate theory applied to functionally graded plates using a meshless method. Mech Adv Mater Struct 17:108–133. https://doi.org/10.1080/15376490903249925
25. Li SL, Liu KY, Long SY, Li GY (2011) The natural neighbor Petrov–Galerkin method for thick plates. Eng Anal Bound Elem 35:616–622. https://doi.org/10.1016/j.enganabound.2010.11.003
26. Zienkiewicz OC, Taylor RL (2000) The finite element method, vol 1. BH Publications, Clarens, Oxford, England
27. Babuska I, Rheinboldt WC (1978) A posteriori error estimates for the finite element method. Int J Numer Methods Eng 12:1597–1615. https://doi.org/10.1002/nme.1620121010

28. Zienkiewicz OC, Zhu JZ (1987) A simple error estimator and adaptive procedure for practical engineering analysis. Int J Numer Methods Eng 24:337–357. https://doi.org/10.1002/nme.1620240206
29. Mohite PH, Upadhyay CS (2002) Local quality of smoothening based a posteriori error estimator for laminated plates under transverse loading. Comput Struct 80:1447–1488. https://doi.org/10.1016/S0045-7949(02)00099-8
30. Mohite PM, Upadhyay CS (2003) Focused adaptivity for laminated plates. Comput Struct 81:287–298. https://doi.org/10.1016/S0045-7949(02)00448-0
31. Mohite PM, Upadhyay CS (2006) Accurate computation of critical local quantities in composite laminated plates under transverse loading. Comput Struct 84:657–675. https://doi.org/10.1016/j.compstruc.2005.11.004
32. Mohite PM, Upadhyay CS (2007) Region by region modeling of laminated composite plates. Comput Struct 85:1808–1827. https://doi.org/10.1016/j.compstruc.2007.04.005
33. Tabarraei A, Sukumar N (2005) Adaptive computation on conforming quadtree meshes. Finite Elem Anal Des 41:686–702. https://doi.org/10.1016/j.finel.2004.08.002
34. Ullah Z, Augarde CE (2013) Finite deformation elasto-plastic modeling using an adaptive meshless method. Comput Struct 118:39–52. https://doi.org/10.1016/j.compstruc.2012.04.001
35. Cai Y, Zhu H (2004) A meshless local natural neighbor interpolation method for stress analysis of solids. Eng Anal Bound Elem 28:607–613. https://doi.org/10.1016/j.enganabound.2003.10.001
36. Yvonnet J, Coffignal G, Ryckelynck D, Lorong P, Chinesta F (2006) A simple error indicator for meshfree methods based on natural neighbors. Comput Struct 84:1301–1312. https://doi.org/10.1016/j.compstruc.2006.04.002
37. Madhukar S, Rajagopal A (2014) Meshless natural neighbor Galerkin method for the bending and vibration analysis of composite plates. Compos Struct 111:138–146. https://doi.org/10.1016/j.compstruct.2013.12.023
38. Mohite PM, Upadhyay CS (2015) Adaptive finite element based shape optimization in laminated composite plates. Comput Struct 153:19–35. https://doi.org/10.1016/j.compstruc.2015.02.020
39. Stein E, Rüter M, Ohnimus S (2004) Adaptive finite element analysis and modelling of solids and structures. Findings, problems and trends. Int J Numer Methods Eng 60(1):103–38. https://doi.org/10.1002/nme.956
40. Stein E, Rüter M, Ohnimus S (2007) Error-controlled adaptive goal-oriented modeling and finite element approximations in elasticity. Comput Methods Appl Mech Eng 196(37):3598–3613. https://doi.org/10.1016/j.cma.2006.10.032
41. Rüter M, Stein E (2006) Goal-oriented a posteriori error estimates in linear elastic fracture mechanics. Comput Methods Appl Mech Eng 15(4):251–278. https://doi.org/10.1016/j.cma.2004.05.032 195) .
42. Roylance D (2001) Introduction to fracture mechanics. Massachusetts Institute of Technology, Cambridge, pp 1–2